

Realizing Three-Electron Redox Reactions in NASICON-Structured $\text{Na}_3\text{MnTi}(\text{PO}_4)_3$ for Sodium-Ion Batteries

Ting Zhu, Ping Hu, Xuanpeng Wang, Zhenhui Liu, Wen Luo, Kwadwo Asare Owusu, Weiwei Cao, Changwei Shi, Jiantao Li, Liang Zhou,* and Liqiang Mai*

Developing multielectron reaction electrode materials is essential for achieving high specific capacity and high energy density in secondary batteries; however, it remains a great challenge. Herein, $\text{Na}_3\text{MnTi}(\text{PO}_4)_3/\text{C}$ hollow microspheres with an open and stable NASICON framework are synthesized by a spray-drying-assisted process. When applied as a cathode material for sodium-ion batteries, the resultant $\text{Na}_3\text{MnTi}(\text{PO}_4)_3/\text{C}$ microspheres demonstrate fully reversible three-electron redox reactions, corresponding to the $\text{Ti}^{3+/4+}$ (≈ 2.1 V), $\text{Mn}^{2+/3+}$ (≈ 3.5 V), and $\text{Mn}^{3+/4+}$ (≈ 4.0 V vs Na^+/Na) redox couples. In situ X-ray diffraction results reveals that both solid-solution and two-phase electrochemical reactions are involved in the sodiation/desodiation processes. The high specific capacity (160 mAh g^{-1} at 0.2 C), outstanding cyclability ($\approx 92\%$ capacity retention after 500 cycles at 2 C), and the facile synthesis make the $\text{Na}_3\text{MnTi}(\text{PO}_4)_3/\text{C}$ a prospective cathode material for sodium-ion batteries.

The low cost and high abundance of sodium resources make sodium-ion batteries (SIBs) one of the most prospective choices for stationary energy storage.^[1–10] However, the insertion/extraction of Na^+ with a radius of 95 pm is usually accompanied by a large volume change, making the development of stable SIB electrode materials a great challenge.^[11–14] In addition, the solid-state diffusion of Na^+ with large radius in electrode materials usually suffers from sluggish kinetics.

Na superionic conductor (NASICON) compounds have the general formula of $\text{A}_x\text{MM}'(\text{XO}_4)_3$ ($\text{A} = \text{Li}, \text{Na}, \text{K}, \text{etc.}; \text{M}, \text{M}' = \text{Fe}, \text{Co}, \text{Ni}, \text{Ti}, \text{V}, \text{etc.}; \text{X} = \text{Si}, \text{P}, \text{S}, \text{As}, \text{etc.}$). With stable 3D framework and large tunnels for Na^+ diffusion and accommodation, NASICON compounds have been considered as an attractive family of electrode materials for SIBs.^[15–20]

T. Zhu, P. Hu, X. P. Wang, Z. H. Liu, Dr. W. Luo, K. A. Owusu, C. W. Shi, J. T. Li, Prof. L. Zhou, Prof. L. Q. Mai
State Key Laboratory of Advanced Technology for Materials
Synthesis and Processing
Wuhan University of Technology
Wuhan 430070, P. R. China
E-mail: liangzhou@whut.edu.cn; mlq518@whut.edu.cn

W. W. Cao

UPR3079 CEMHTI

1D Avenue de la Recherche Scientifique, 45071 Orléans Cedex 2, France

 The ORCID identification number(s) for the author(s) of this article can be found under <https://doi.org/10.1002/aenm.201803436>.

DOI: 10.1002/aenm.201803436

$\text{Na}_3\text{V}_2(\text{PO}_4)_3$ represents a well-known NASICON-structured SIB cathode. It possesses a theoretical capacity of 117 mAh g^{-1} with a discharge plateau at ≈ 3.4 V. Besides $\text{Na}_3\text{V}_2(\text{PO}_4)_3$, NASICON-structured $\text{Na}_3\text{MnTi}(\text{PO}_4)_3$,^[21,22] $\text{Na}_2\text{VTi}(\text{PO}_4)_3$,^[23,24] $\text{Na}_4\text{MnV}(\text{PO}_4)_3$,^[25–27] $\text{Na}_3\text{MgTi}(\text{PO}_4)_3$,^[28] $\text{Na}_{1+x}\text{Fe}_x\text{Ti}_{2-x}(\text{PO}_4)_3$,^[29] $\text{Na}_3\text{FeV}(\text{PO}_4)_3$,^[25] and $\text{Na}_4\text{NiV}(\text{PO}_4)_3$ ^[25,30] have also been studied in sodium storage. It should be mentioned that the number of electrons involved in the electrochemical reactions for all the above-mentioned NASICON-structured compounds is limited to 2 per formula. Exploring NASICON-structured cathode materials with three-electron redox reactions and excellent cyclability has been demonstrated to be a grand challenge.

Recently, Gao et al. reported the NASICON-structured $\text{Na}_3\text{MnTi}(\text{PO}_4)_3$ with fully reversible $\text{Mn}^{2+/3+}$ (≈ 3.6 V vs Na^+/Na) and $\text{Mn}^{3+/4+}$ (≈ 4.1 V vs Na^+/Na) redox couples in organic electrolytes.^[21] In aqueous electrolyte, the $\text{Na}_3\text{MnTi}(\text{PO}_4)_3$ showed the reversible redox couples of $\text{Mn}^{2+/3+}$ and $\text{Ti}^{3+/4+}$ in the positive and negative potential windows, respectively.^[22] However, the simultaneous realization of $\text{Ti}^{3+/4+}$, $\text{Mn}^{2+/3+}$, and $\text{Mn}^{3+/4+}$ redox couples in either organic or aqueous electrolyte has not been demonstrated yet.

Herein, we produced $\text{Na}_3\text{MnTi}(\text{PO}_4)_3/\text{C}$ (NMTP/C) hollow microspheres by a spray-drying-assisted method. Interestingly, the resultant NMTP/C demonstrates fully reversible three-electron redox reactions at 2.1, 3.5, and 4.0 V vs Na^+/Na , corresponding to the $\text{Ti}^{3+/4+}$, $\text{Mn}^{2+/3+}$, and $\text{Mn}^{3+/4+}$ redox couples, respectively. The reversible three-electron redox reactions endow the NMTP/C a high specific capacity of 160 mAh g^{-1} at 0.2 C. The stable and open NASICON framework ensures the superior cycling stability of NMTP/C (90% capacity retention after 500 cycles at 2 C). In situ X-ray diffraction (XRD) result reveals that both solid-solution and two-phase electrochemical reactions are involved in the sodium storage processes. NMTP/C-650/carbon Na-ion full cells are also assembled, manifesting a specific capacity of 139 mAh g^{-1} (based on the mass of cathode materials) at 0.5 C.

The NMTP/C microspheres are synthesized by a scalable spray-drying-assisted process followed by annealing in Ar. XRD Rietveld analysis (Figure 1a) reveals that NMTP/C-650 adopts a rhombohedral NASICON-type structure with a space group of $R\bar{3}c$. The refined profiles fit well with the experimental

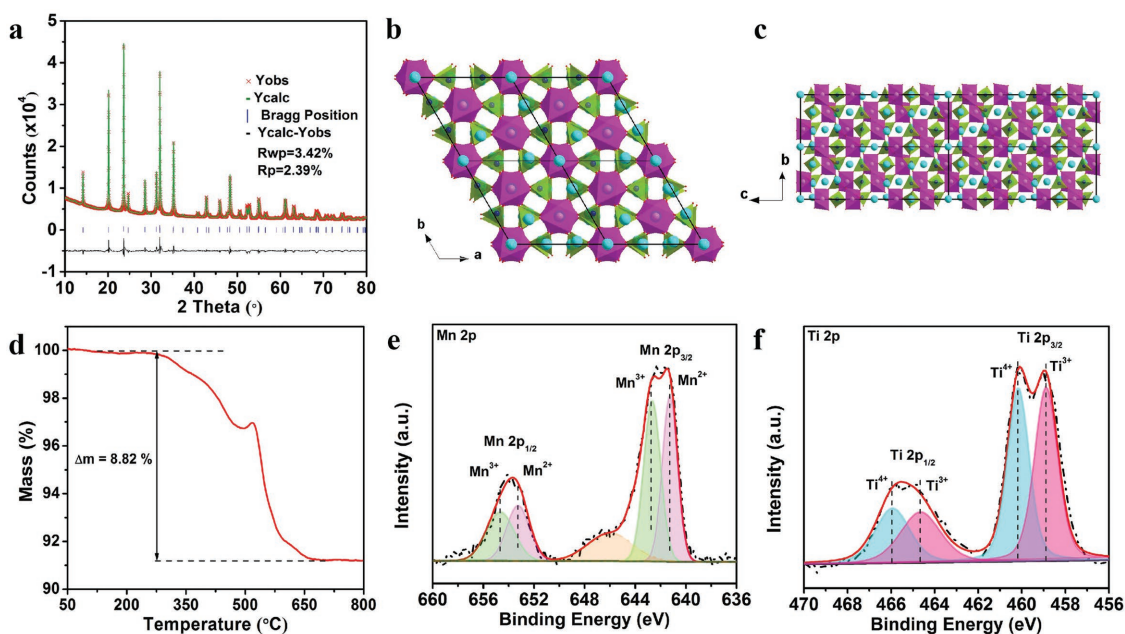


Figure 1. a) Rietveld refinement of the NASICON-structured NMTP/C-650 and b,c) the schematic structure of $\text{Na}_3\text{MnTi}(\text{PO}_4)_3$. The MnO_6 and TiO_6 octahedra are presented in magenta, the PO_4 octahedra are in green, and the sodium ions are in cyan. d) TGA curve, and e) high-resolution Mn 2p and f) Ti 2p XPS spectra of NMTP/C-650.

data, and the unit cell parameters obtained from the structural refinement are $a = 8.8343 \text{ \AA}$ and $c = 21.6654 \text{ \AA}$ (Table S1, Supporting Information). The intense and sharp diffraction peaks indicate that the sample has a high crystallinity. The NMTP is constructed by isolated TiO_6 and MnO_6 octahedra sharing all the corners with PO_4 tetrahedra (Figure 1b,c). The polyanionic phosphate framework endows the $\text{Na}_3\text{MnTi}(\text{PO}_4)_3$ excellent structural stability and intrinsic safety.

Thermogravimetric analysis (TGA) is carried out in the air to determine the carbon content of the sample (Figure 1d). The total weight loss for NMTP/C-650 is 8.82 wt%. A slight mass increase happens at $\approx 520 \text{ }^\circ\text{C}$, which is due to the oxidation of low-valence-state metal species. Considering the oxidation of the metal species during the combustion of carbon, the actual carbon contents of NMTP/C-650 should be slightly higher than the total weight loss (8.82 wt%). From the CHNS analysis, the carbon content of NMTP/C-650 is 8.85 wt%, which is consistent with the TGA result (Table S2, Supporting Information). Raman spectrum of NMTP/C-650 shows two characteristic peaks for carbon at 1350 cm^{-1} (D-band) and 1594 cm^{-1} (G-band) (Figure S3, Supporting Information). The I_D/I_G ratio of NMTP/C-650 is 0.90, indicating that the carbon is partially graphitized.

The surface valence states of Mn and Ti are investigated by X-ray photoelectron spectroscopy (XPS) (Figure 1e,f). According to a recent publication, the Mn and Ti exist as Mn^{2+} and Ti^{4+} in the NASICON-structured $\text{Na}_3\text{MnTi}(\text{PO}_4)_3$.^[22] Interestingly, we find that a non-negligible fraction of Mn^{3+} ($[\text{Mn}^{3+}]/([\text{Mn}^{3+}] + [\text{Mn}^{2+}]) = 52.01\%$) exists in the sample. Accompanying the existence of Mn^{3+} , a significant fraction of Ti^{3+} ($[\text{Ti}^{3+}]/([\text{Ti}^{3+}] + [\text{Ti}^{4+}]) = 51.67\%$) is also observed.

Figure 2 shows the detailed microstructure of as-synthesized NMTP/C-650. The NMTP/C-650 is composed of microspheres with diameters ranging from 0.2 to 5 μm (Figure 2a,b).

Transmission electron microscopy (TEM) image (Figure 2c) demonstrates that the NMTP/C-650 microspheres possess hollow interiors. Such a hollow structure with thin shell thickness would short the Na^+ diffusion distance when applied in SIBs. The high-resolution TEM (HRTEM) image shows the interplanar spacings of 0.44 nm, which matches well with the (104) planes of NMTP (Figure 2d).^[21,22] The high-angle annular dark-field scanning TEM (HAADF-STEM) image further confirms the hollow microspherical structure of NMTP/C-650 (Figure 2e). The energy-dispersive spectroscopy (EDS) mappings (Figure 2f) demonstrate that the Mn, Ti, C, Na, O, and P are homogeneously distributed in the NMTP/C-650 composite hollow spheres. For comparison, NMTP/C-600 and NMTP/C-700 (Figures S1–S8, Supporting Information) are also prepared by varying the annealing temperature.

To study the theoretical sodium storage capacity of NMTP/C-650, galvanostatic intermittent titration technique (GITT) measurement is conducted (Figure 3a). The cell is charged to 4.2 V at 50 mA g^{-1} before GITT test.^[31,32] The NMTP/C-650 delivers a discharge capacity of 173 mAh g^{-1} in GITT test, corresponding to $\approx 2.95 \text{ Na}^+$ intercalated into NMTP per formula (see Supporting Information). The discharge plateaus are located at 4.01, 3.52, and 2.12 V, corresponding to the reduction of Mn^{4+} to Mn^{3+} , Mn^{3+} to Mn^{2+} , and Ti^{4+} to Ti^{3+} , respectively.

Cyclic voltammetry (CV) is also employed to study the sodium storage performance of NMTP/C-650. Three pairs of redox peaks located at 2.21/2.05, 3.75/3.44, and 4.15/3.94 V can be observed in the first cycle (Figure 3b), corresponding to the redox couples of $\text{Ti}^{3+/4+}$, $\text{Mn}^{2+/3+}$, and $\text{Mn}^{3+/4+}$, respectively.^[21,22] An additional pair of redox peaks with weak intensities can be observed at 2.43/2.33 V in the subsequent cycles. Unfortunately, these peaks cannot be assigned to any known redox couples at this stage.

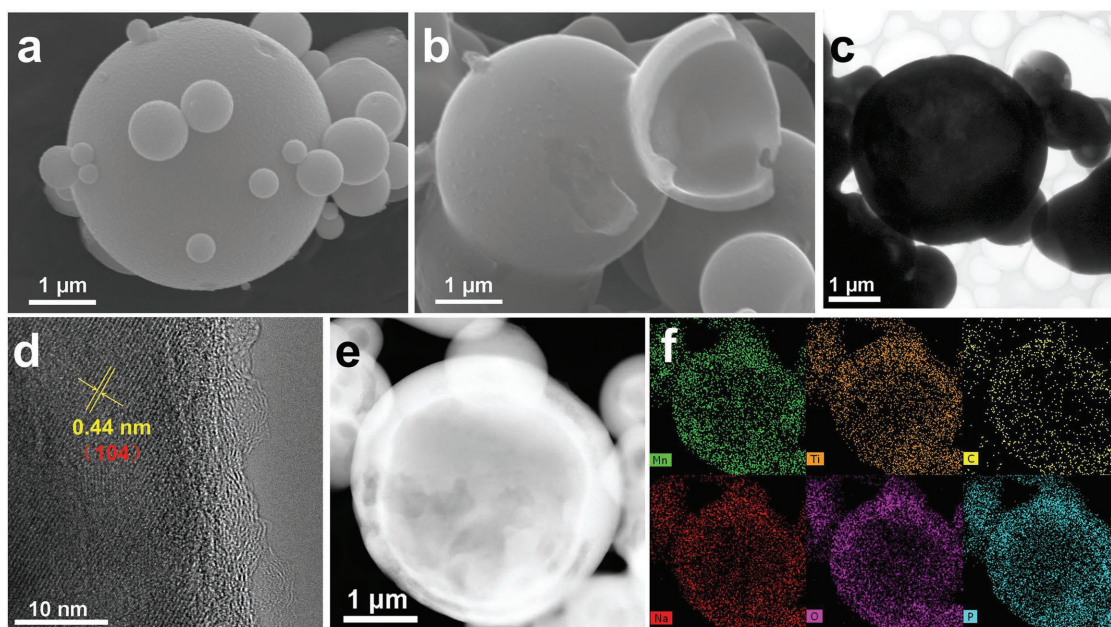


Figure 2. a,b) SEM, c) TEM, and d) HRTEM images of NMTP/C-650; e) HAADF-STEM image of NMTP/C-650 and f) the corresponding elemental mappings of manganese (green), titanium (orange), carbon (yellow), sodium (red), oxygen (purple), and phosphorus (blue).

Figure 3c presents the charge/discharge curves of NMTP/C-650 under various C-rates. Obvious plateaus can be discerned from the charge/discharge curves, which is consistent with the CV results. The NMTP/C-650 delivers discharge capacities of 160, 150, 141, and 129 mAh g^{-1} at 0.2, 0.5, 1, and 2 C, respectively (Figure 3c). In addition, the discharge capacity of NMTP/C-650 can be fully recovered when the C-rate is reduced back to 0.2 C after the high-rate test (Figure 3d). Obviously,

the NMTP/C-650 outperforms the NMTP/C-600 and NMTP/C-700 in terms of specific discharge capacity and rate capability (Figure 3d; Figures S9 and S10, Supporting Information). When cycled at 2 C, the NMTP/C-650 exhibits a high discharge capacity of 119 mAh g^{-1} , and $\approx 92\%$ capacity retention can be observed after 500 cycles (Figure 3e,f). Under the same conditions, the NMTP/C-600 and NMTP/C-700 exhibit much lower discharge capacities and capacity retentions.

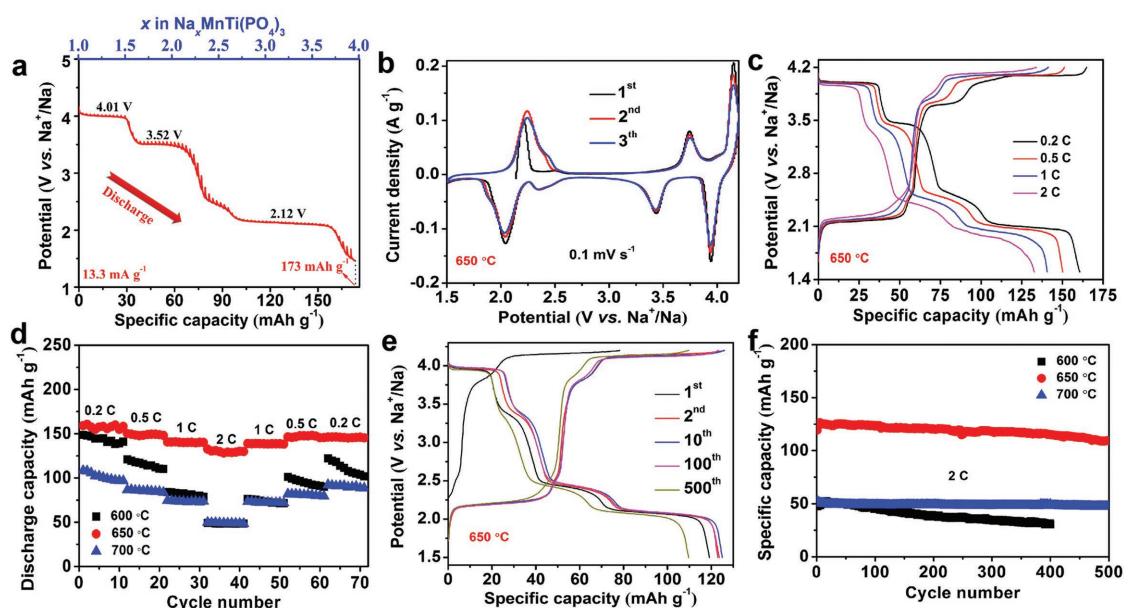


Figure 3. a) The GITT curve of NMTP/C-650 at a current density of 13.3 mA g^{-1} in a discharged process. b) CV profiles of NMTP/C-650 at a scan rate of 0.1 mV s^{-1} in the electrochemical window of 1.5–4.2 V vs Na^+/Na . c) Charge/discharge curves of NMTP/C-650 at different rates. d) Rate performances of NMTP/C-600, NMTP/C-650, and NMTP/C-700. e) Representative charge/discharge curves of NMTP/C-650 at 2 C. f) Cycling performances of NMTP/C-600, NMTP/C-650, and NMTP/C-700 at 2 C.

To the best of our knowledge, the sodium storage performances of NMTP/C-650 are superior to most of the recently reported NASICON-structured SIB cathode materials (Table S3, Supporting Information). Electrochemical impedance spectroscopy (EIS) was used to study the electron/ion diffusion dynamics of the NMTP/C (Figure S11, Supporting Information). The equivalent electrical circuit for fitting the impedance data is shown in the inset of Figure S11 in the Supporting Information^[27,33–35] and the fitting results are summarized in Table S4 in the Supporting Information. The NMTP/C-650 manifests the lowest charge transfer resistance and the highest Na^+ diffusion coefficient, which is responsible for its superior sodium storage performances.

To elucidate the structural change of NMTP/C-650 during the sodiation/desodiation processes, in situ XRD test is performed. In general, the diffraction peaks located at $20\text{--}21^\circ$, $23\text{--}24.5^\circ$, $27.5\text{--}29^\circ$, $30\text{--}33^\circ$, and $34\text{--}36^\circ$ undergo a series of obvious and reversible changes during charge/discharge, demonstrating the highly reversible electrochemical reactions (Figure 4a). Specifically, the (211) (at $\approx 30.5^\circ$) and (116) (at $\approx 34.5^\circ$) diffractions shift rightward and then disappear during the desodiation process. Both peaks appear at the later stage of sodiation process and then shift leftward. The reversible peak shift indicates a solid-solution reaction, while the disappearance/appearance of

diffraction peaks suggests a two-phase reaction.^[4] That is to say, both solid-solution and two-phase reactions are involved in the sodium storage process of NMTP/C-650. Based on the electrochemical characterizations, the structure evolution of NMTP during the sodium intercalation/deintercalation processes is proposed (Figure 4b). During the first desodiation process, two Na^+ deintercalate from NMTP. Upon subsequent sodiation/desodiation, three Na^+ reversibly intercalate into and deintercalate from the NMTP framework.

Na-ion full cells are also assembled based on the NMTP/C-650 cathode and a soft carbon anode (Figures S12–S14, Supporting Information). The full cell displays a specific capacity of 139 mAh g^{-1} (based on the mass of NMTP/C-650) at 0.5 C , retaining 117 mAh g^{-1} after 50 cycles (Figure S15, Supporting Information). The results demonstrate the practical applicability of NMTP/C-650 in sodium storage.

In summary, NMTP/C microspheres are produced by a spray-drying-assisted method. Unlike most NASICON-structured cathode materials, the NMTP/C demonstrates fully reversible three-electron redox reactions at 2.1, 3.5, and 4.0 V vs Na^+/Na , corresponding to the $\text{Ti}^{3+/4+}$, $\text{Mn}^{2+/3+}$, and $\text{Mn}^{3+/4+}$ redox couples, respectively. The reversible three-electron redox reactions endow the NMTP/C a high specific capacity of 160 mAh g^{-1} at

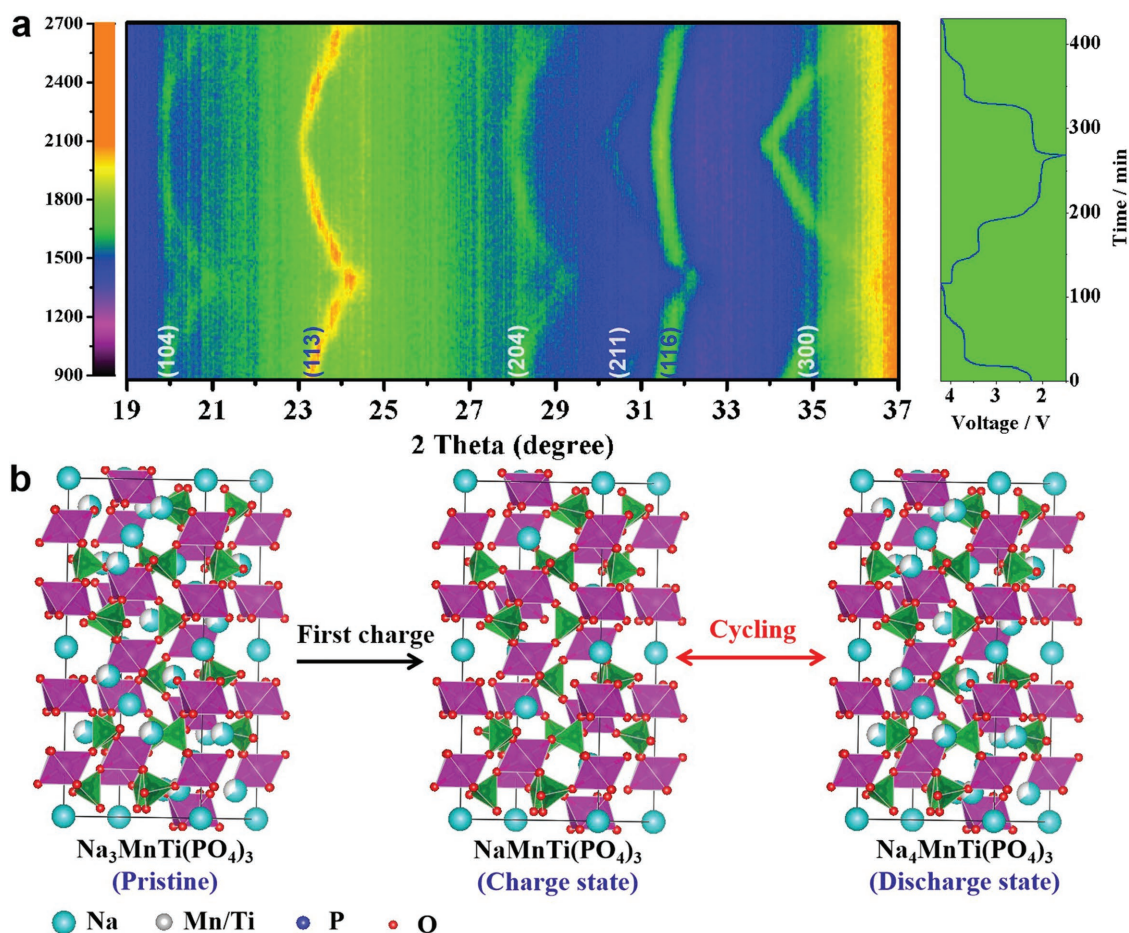


Figure 4. a) In situ XRD patterns of the NMTP/C-650 collected during galvanostatic charge/discharge at 50 mA g^{-1} . b) Schematic illustration showing 2 Na^+ deintercalating from $\text{Na}_3\text{MnTi}(\text{PO}_4)_3$ during the first charge process, and 3 Na^+ intercalating into/deintercalating from the framework upon subsequent electrochemical discharge/charge processes.

0.2 C, and the highly stable NASICON framework ensures the superior cycling stability of NMTP/C ($\approx 92\%$ capacity retention after 500 cycles at 2 C). In situ XRD characterization reveals that the sodium storage in NMTP/C involves both solid-solution and two-phase reactions. This work sheds light on the rational design of NASICON-structured cathode materials for realizing multielectron redox reactions per transition metal.

Experimental Section

Materials Synthesis: The NMTP/C-650 microspheres were synthesized by a facile spray-drying method with postannealing. In a typical synthesis, NaH_2PO_4 (15 mmol), $\text{Mn}(\text{CH}_3\text{COO})_2 \cdot 4\text{H}_2\text{O}$ (5 mmol), dihydroxybis(ammonium lactato)titanium(IV) ($\text{C}_6\text{H}_{18}\text{N}_2\text{O}_8\text{Ti}$, 5 mmol), and citric acid (10 mmol) were dissolved in deionized water and stirred at room temperature for 30 min. Next, the solution was spray-dried using a BUCHI Mini Spray Dryer B-290 to prepare the NMTP/C precursor. The detailed conditions during spray drying were listed as follows: inlet temperature 220 °C, aspirator rate 90%, rotameter setting 40 mm, and pump rate 5%. The NMTP/C-650 was obtained after annealing the precursor at 650 °C for 4 h in Ar. NMTP/C-600 and NMTP/C-700 were prepared by the same procedure, except the annealing temperatures were set at 600 and 700 °C, respectively.

Structure Characterization: XRD measurements were performed on a Bruker D8 Discover X-ray diffractometer with a nonmonochromated $\text{Co K}\alpha$ X-ray source ($\lambda = 1.5406 \text{ \AA}$). TGA was performed on a STA-449C thermobalance in the air with a temperature ramp of $5 \text{ }^\circ\text{C min}^{-1}$. The CHNS elemental analysis was performed with an elemental analyzer (Vario EL cube, Elementar Analysensysteme, Germany). XPS analysis was performed using a VG Multilab 2000. Raman spectra were recorded with a Renishaw INVIA Raman microscope with an Ar 514.5 nm laser. Field-emission scanning electron microscopy images were collected using a JEOL-7100F microscope. TEM, HRTEM, and HAADF-STEM images were recorded using a JEOL JEM-2100F STEM/EDS microscope working at 200 kV.

Electrochemical Characterization: The electrochemical properties were performed with 2016 coin-type cells in an Ar-filled glove box. The cathode was fabricated by pressing a slurry containing active material (70 wt%), acetylene black (20 wt%), and polyvinylidene fluoride (10 wt%) in *N*-methyl-2-pyrrolidone onto an aluminum foil and dried under vacuum at 70 °C for 12 h. The loading mass of the active material was $\approx 1.2\text{--}1.8 \text{ mg cm}^{-2}$. Sodium disks were employed as the counter and reference electrodes, 1 M NaClO_4 in ethylene carbon/propylene carbonate (1:1 w/w) with 5% fluoroethylene carbonate (electrolyte additive) was used as the electrolyte, and Whatman glass microfiber paper was used as the separator. Galvanostatic charge/discharge tests were performed in the potential window of 1.5–4.0 V vs Na/Na^+ using a multichannel battery testing system (LAND CT2001A). CV and EIS were conducted using CHI600E and Autolab PGSTAT 302N electrochemical workstations. For GITT measurements, the cell was discharged at 13.3 mA g^{-1} for 10 min on each current step; a relaxation time of 10 min was set between two successive current steps to allow the cell reach quasi-equilibrium state.

In situ XRD experiments during electrochemical testing were performed on a D8 Discover X-ray diffractometer equipped with a planar detector. The cathode containing active material (60 wt%), acetylene black (30 wt%), and polytetrafluoroethylene (10 wt%) was cut into square slices with an area of $\approx 1 \text{ cm}^2$ and a thickness of $\approx 0.15 \text{ mm}$. The cathode was placed on the back side of an X-ray transparent Be window that also served as the current collector. The in situ XRD signals were collected in the 2θ range of $19\text{--}37^\circ$ with a still mode during the charge/discharge processes; each pattern was acquired in 120 s.

Supporting Information

Supporting Information is available from the Wiley Online Library or from the author.

Acknowledgements

This work was supported by the National Natural Science Foundation of China (21673171 and 51502226) and the National Key Research and Development Program of China (2018YFB010420 and 2016YFA0202603).

Conflict of Interest

The authors declare no conflict of interest.

Keywords

cathode materials, $\text{Na}_3\text{MnTi}(\text{PO}_4)_3$, NASICON structure, sodium-ion batteries, three-electron redox reactions

Received: November 7, 2018

Revised: December 17, 2018

Published online:

- [1] N. Yabuuchi, K. Kubota, M. Dahbi, S. Komaba, *Chem. Rev.* **2014**, *114*, 11636.
- [2] H. S. Li, L. L. Peng, Y. Zhu, D. H. Chen, X. G. Zhang, G. H. Yu, *Energy Environ. Sci.* **2016**, *9*, 3399.
- [3] G. L. Xu, Z. H. Chen, G. M. Zhong, Y. Z. Liu, Y. Yang, T. Y. Ma, Y. Ren, X. B. Zuo, X. H. Wu, X. Y. Zhang, K. Amine, *Nano Lett.* **2016**, *16*, 3955.
- [4] Y. Sun, L. Zhao, H. L. Pan, X. Lu, L. Gu, Y. S. Hu, H. Li, M. Armand, Y. C. Ikuhara, L. Q. Chen, X. J. Huang, *Nat. Commun.* **2013**, *4*, 1870.
- [5] B. Zhang, G. Rousse, D. Foix, R. Dugas, D. A. D. Corte, J. M. Tarascon, *Adv. Mater.* **2016**, *28*, 9824.
- [6] X. S. Wang, D. Chen, Z. H. Yang, X. H. Zhang, C. Wang, J. T. Chen, X. X. Zhang, M. Q. Xue, *Adv. Mater.* **2016**, *28*, 8645.
- [7] J. Liu, L. T. Yu, C. Wu, Y. R. Wen, K. B. Yin, F. K. Chiang, R. Z. Hu, J. W. Liu, L. T. Sun, L. Gu, J. Maier, Y. Yu, M. Zhu, *Nano Lett.* **2017**, *17*, 2034.
- [8] Y. S. Wang, R. J. Xiao, Y. S. Hu, M. Avdeev, L. Q. Chen, *Nat. Commun.* **2015**, *6*, 6954.
- [9] F. P. Zhao, S. D. Shen, L. Cheng, L. Ma, J. H. Zhou, H. L. Ye, N. Han, T. P. Wu, Y. G. Li, J. Lu, *Nano Lett.* **2017**, *17*, 4137.
- [10] L. Wang, Y. H. Lu, J. Liu, M. W. Xu, J. G. Cheng, D. W. Zhang, J. B. Goodenough, *Angew. Chem.* **2013**, *125*, 2018.
- [11] Y. N. Xu, Q. L. Wei, C. Xu, Q. D. Li, Q. Y. An, P. F. Zhang, J. Z. Sheng, L. Zhou, L. Q. Mai, *Adv. Energy Mater.* **2016**, *6*, 1600389.
- [12] N. O. Vitoriano, N. E. Drewett, A. Gonzalo, T. Rojo, *Energy Environ. Sci.* **2017**, *10*, 1051.
- [13] P. Singh, K. Shiva, H. Celio, J. B. Goodenough, *Energy Environ. Sci.* **2015**, *8*, 3000.
- [14] J. Billaud, R. J. Clément, A. R. Armstrong, J. C. Vázquez, P. Rozier, C. P. Grey, P. G. Bruce, *J. Am. Chem. Soc.* **2014**, *136*, 17243.
- [15] S. Li, Y. F. Dong, L. Xu, X. Xu, L. He, L. Q. Mai, *Adv. Mater.* **2014**, *26*, 3545.
- [16] R. Rajagopalan, B. Chen, Z. C. Zhang, X. L. Wu, Y. H. Du, Y. Huang, B. Li, Y. Zong, J. Wang, G. H. Nam, M. Sindoro, S. X. Dou, H. K. Liu, H. Zhang, *Adv. Mater.* **2017**, *29*, 1605694.
- [17] C. Xu, Y. N. Xu, C. J. Tang, Q. L. Wei, J. S. Meng, L. Huang, L. Zhou, G. B. Zhang, L. He, L. Q. Mai, *Nano Energy* **2016**, *28*, 224.
- [18] Y. J. Fang, L. F. Xiao, J. F. Qian, Y. L. Cao, X. P. Ai, Y. H. Huang, H. X. Yang, *Adv. Energy Mater.* **2016**, *6*, 1502197.
- [19] X. P. Wang, C. J. Niu, J. S. Meng, P. Hu, X. M. Xu, X. J. Wei, L. Zhou, K. N. Zhao, W. Luo, M. Y. Yan, L. Q. Mai, *Adv. Energy Mater.* **2015**, *5*, 1500716.

- [20] C. B. Zhu, K. P. Song, P. A. Aken, J. Maier, Y. Yu, *Nano Lett.* **2014**, *14*, 2175.
- [21] H. C. Gao, Y. T. Li, K. Park, J. B. Goodenough, *Chem. Mater.* **2016**, *28*, 6553.
- [22] H. C. Gao, J. B. Goodenough, *Angew. Chem.* **2016**, *128*, 12960.
- [23] H. B. Wang, T. R. Zhang, C. Chen, M. Ling, Z. Lin, S. Q. Zhang, F. Pan, C. D. Liang, *Nano Res.* **2018**, *11*, 490.
- [24] J. Dong, G. M. Zhang, X. G. Wang, S. Zhang, C. Deng, *J. Mater. Chem. A* **2017**, *5*, 18725.
- [25] W. D. Zhou, L. G. Xue, X. J. Lü, H. C. Gao, Y. T. Li, S. Xin, G. T. Fu, Z. M. Cui, Y. Zhu, J. B. Goodenough, *Nano Lett.* **2016**, *16*, 7836.
- [26] F. Chen, V. M. Kovrugin, D. Régnal, O. Mentré, F. François, C. Jean-Noël, M. Christian, *Small Methods* **2018**, <https://doi.org/10.1002/smt.201800218>.
- [27] H. X. Li, T. Jin, X. B. Chen, Y. Q. Lai, Z. A. Zhang, W. Z. Bao, L. F. Jiao, *Adv. Energy Mater.* **2018**, *8*, 1801418.
- [28] F. Zhang, W. F. Li, X. D. Xiang, M. L. Sun, *Chem. Eur. J.* **2017**, *23*, 12944.
- [29] M. J. Aragón, C. Vidal-Abarca, P. Lavela, J. L. Tirado, *J. Power Sources* **2014**, *252*, 208.
- [30] H. Li, Y. Bai, F. Wu, Q. Ni, C. Wu, *ACS Appl. Mater. Interfaces* **2016**, *8*, 27779.
- [31] Y. H. Xu, Y. J. Zhu, Y. H. Liu, C. S. Wang, *Adv. Energy Mater.* **2013**, *3*, 128.
- [32] D. W. Dees, S. Kawauchi, D. P. Abraham, J. Parkash, *J. Power Sources* **2009**, *189*, 263.
- [33] L. Li, M. Xu, Q. Yao, Z. Chen, L. Song, Z. Zhang, C. Gao, P. Wang, Z. Yu, Y. Lai, *ACS Appl. Mater. Interfaces* **2016**, *8*, 30879.
- [34] M. V. Reddy, G. V. Subba Rao, B. V. Chowdari, *Chem. Rev.* **2013**, *113*, 5364.
- [35] M. V. Reddy, G. V. Subba Rao, B. V. Chowdari, *J. Mater. Chem.* **2011**, *21*, 10003.